A ghost-stabilised material point method for large deformation geotechnical analysis

W.M. Coombs[1]

[1]Department of Engineering, Durham University, Durham, UK

ABSTRACT: The Material Point Method (MPM) is *advertised* as *the* method for large deformation analysis of geotechnical problems. However, the method suffers from several instabilities which are widely documented in the literature, such as: material points crossing between elements, different number of points when projecting quantities between the grid and points, etc. A key issue that has received relatively little attention in the literature is the conditioning of the linear system of equations due to the arbitrary nature of the interaction between the physical body (represented by material points) and the background grid (used to solve the governing equations). This arbitrary interaction can cause significant issues when solving the linear system, making some systems unsolvable or causing them to predict spurious results. This paper presents a cut-FEM (Finite Element Method) inspired ghost-stabilised MPM that removes this issue.

Keywords: Numerical Analysis; Material Point Method; Large Deformation Mechanics; Stabilisation; Non-Matching Mesh Methods

1 INTRODUCTION

The Material Point Method (MPM, Sulsky *et al.*, 1994) developed from Particle In Cell (PIC) and FLuid Implicit Particle (FLIP) approaches as a large deformation analysis approach for solid mechanics. The core idea behind the method is to decouple the physical deformation of the material from the underlying background mesh that is used to solve the governing equations. This allows the method to handle very large deformations whilst avoiding issues such as mesh distortion, remeshing and remapping of material and state variables. The MPM has been widely adopted in both the computational mechanics and computer graphics communities and applied to several areas of geotechnical engineering, such as slope stability and soil-structure interaction.

A well-documented issue with the original MPM is the instability that arises as Material Points (MPs) cross between background grid cells. This so-called cell crossing instability is caused by the sudden transfer of mass and stiffness between elements and, more importantly, the change of sign of the internal force contribution of the crossing material point to the background grid. Several approaches have been proposed to avoid this instability, such as the Generalised Interpolation Material Point Method (GIMPM, Bardenhagen and Kober, 2004), CPDI approaches (Sadeghirad *et al.*, 2011), and B-Spline based MPMs (Yamaguchi *et al.*, 2021). All the approaches remove (or reduce) the instability by increasing the continuity of the basis functions between adjacent elements of the background grid. However, the

MPM (and its variants) suffer from another instability that, at least to date, has received very little attention. This instability is linked to the arbitrary nature of the position of the physical body being analysed relative to the background grid. This can cause very small dependencies (i.e. very small basis function values) to develop between the nodes of the background grid and the MPs. As these dependencies are used to formulate the mass and stiffness matrices, which are used to solve the governing equations on the background grid, the resulting linear system of equations can become ill conditioned, with the associated difficulties in finding a solution and the accuracy of said solution.

This paper presents a cut-Finite Element Method (cut-FEM) inspired approach to overcome this issue via stabilisation of the background grid elements near the boundary of the physical domain, whilst not requiring explicit representation of the physical boundary. The method is applied to a classic geotechnical engineering problem, demonstrating the importance of the stabilisation for robust MP-based simulations.

2 MATERIAL POINT METHOD

As outlined in the introduction, the MPM discretises a physical body (or domain, Ω) via a collection of MPs with associated position, $\{x_p\}$, volume, V_p, mass, m_p, stress, $\{\sigma_p\}$, etc. whilst the governing equations are assembled and solved on the vertices, v, of the background grid. This paper is restricted to solving quasi static solid mechanics stress analysis problems

within an updated Lagrangian finite deformation framework where the governing equations are solved in the current or deformed configuration.

The Galerkin weak statement for equilibrium for each background cell, E, is

$$\int_{\varphi_t(E)} [\nabla_x S_{vp}]^T \{\sigma_p\} dv - \int_{\varphi_t(E)} [S_{vp}]^T \{b\} dv = 0 \quad (1)$$

where φ_t is the motion of the material body, $[S_{vp}]$ and $[\nabla_x S_{vp}]$ contain the basis functions that map information between the MPs and the vertices of the background grid and their spatial derivatives, and $\{b\}$ are the body forces acting over the material volume, v. The Cauchy stress at the MPs, $\{\sigma_p\}$, is based on a linear relationship between logarithmic (or Hencky) strains and Kirchhoff stress and an exponential map of the plastic flow rule to recover the infinitesimal format of elasto-plastic stress update algorithms.

The key steps in an MPM analysis are shown in Figure 1 (ordered top left to bottom right). The total imposed load is split into n time/load steps and the following algorithm followed:

1. The interaction of the physical body, discretised by MPs, and the background grid is determined via evaluation of the basis functions, S_{vp}, of the grid vertices at the MP locations.

2. Information held at the MPs, such as stress, body forces and stiffness, is mapped to the nodes of the background grid using the basis functions and spatial derivatives.

3. The governing equations are assembled on the *active* background grid nodes (that is, at the nodes with non-zero S_{vp} values).

4. The governing equations are solved on the background grid and the incremental displacements of the nodes determined that satisfy the governing equations.

5. Information is mapped from the nodes to the MPs, updating information such as MP positions, deformation, stress, etc.

6. Finally, the background grid is reset (or replaced) and the process repeated.

2.1 Implicit solution

Although the techniques described in this paper can be applied to all variants of the MPM, this paper is focused on quasi-static analysis where the governing equations are solved (Step 4 in the above algorithm) using an implicit Newton-Raphson approach. The implementation is based on the AMPLE (A Material Point Learning Environment) open-source code of Coombs & Augarde (2020), which has its origins in the work of Charlton *et al.* (2017). This solution method

requires the internal force and tangent stiffness to be repeatedly evaluated and used to update the incremental displacements over the load/time step until the discretised weak form statement of equilibrium converges within a given tolerance. A key part of this process is the inversion of the current tangent stiffness matrix (or rather a linear solution involving the tangent stiffness), where the solution accuracy/feasibility is highly dependent on the conditioning of the stiffness matrix.
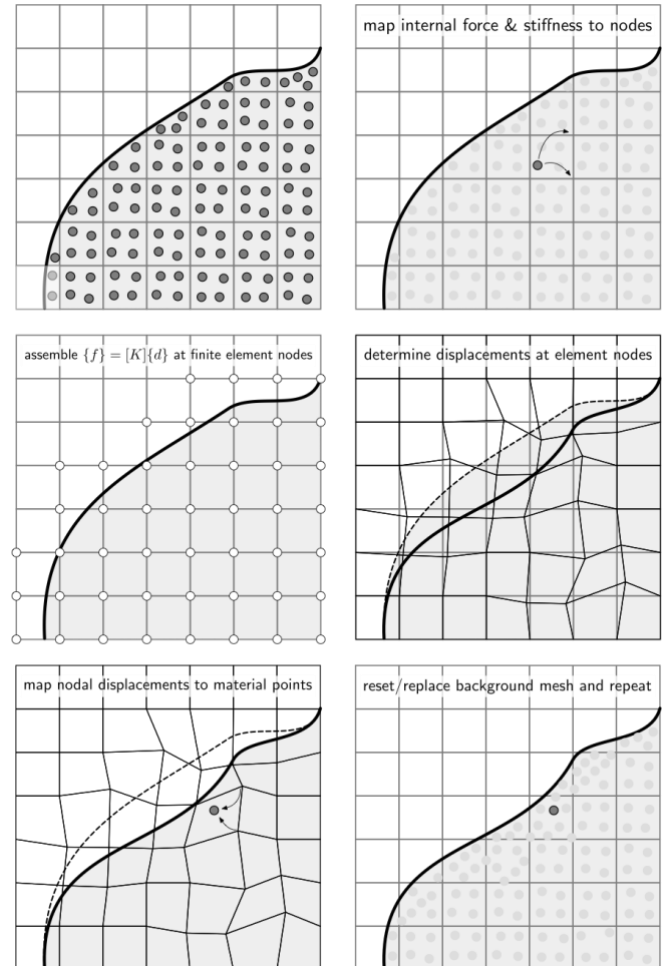

Figure 1. MPM steps (top left to bottom right)

2.2 Conditioning issues

The condition number of a linear system of equations is the ratio of its largest and smallest eigenvalues. For the MPM the intersection between the physical domain (described by the MPs) and the background grid (where the equations are solved) is arbitrary. This can lead to very small overlaps between the domain and some elements, resulting in very small basis function values. The issue is compounded by domain-based MPMs, such as the Generalised Interpolation MPM (GIMPM), where each MP is represented by a rectangular domain and the basis functions are determined by integrating the grid shape functions over each MP domain. Small overlaps between MP domains and elements can

therefore lead to very small S_{vp} and $\nabla_x S_{vp}$ values. These basis functions and their spatial gradients are used to form the mass and stiffness matrices, respectively, leading to unbounded smallest eigenvalues and therefore condition numbers.
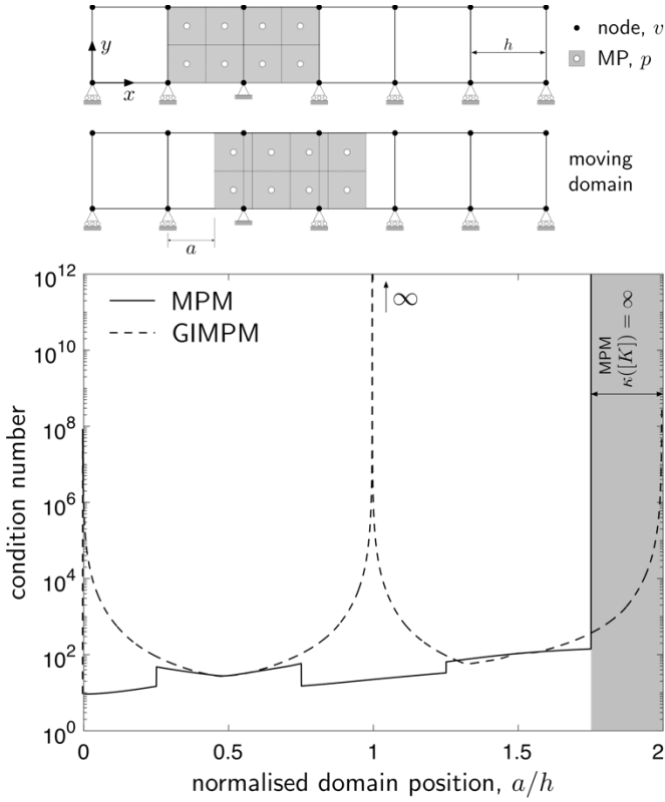

Figure 2. Stiffness matrix condition number

This issue is demonstrated in Figure 2 via a trivial conceptual problem where a MP domain (shown by the shaded region and associated white circles) translates through a background grid (nodes are shown by the back points). The base of the background grid is restrained by a roller boundary condition (zero y displacement) and the node at $x = 2h$ is also restrained in the x direction. In this example the material's Young's modulus was 1Pa, the Poisson's ratio was set to zero and $h = 1$m. The 2×1m physical domain was discretised by eight MPs. Figure 2 provides the condition number, $\kappa([K])$, of the reduced stiffness matrix[1] for the MPM and GIMPM for a translation of $a \in [0,2h]$.

The response of the GIMPM highlights the issue of the unbounded nature of the condition number due to small overlaps between the mesh and the physical domain at $a = h$ and $a = 2h$, where $\kappa([K])$ tends to infinity due to very small $\nabla_x S_{vp}$ values. The condition of the MPM stiffness matrix is bounded until the boundary conditions no longer restrain the x motion of

---

the domain (which is reasonable for any numerical method). However, the standard MPM suffers from several other issues, principally the well documented cell crossing instability. In addition, the condition number of the mass matrix for any MPM is unbounded as the mass matrix is based on the basis functions, which can be arbitrarily small.

3 GHOST STABILISATION

In this paper the *ghost stabilisation* approach (Burman, 2010) is adopted to remedy the condition number issues highlighted in the previous section. The key idea of ghost stabilisation is to enforce additional continuity on the system of equations being solved by penalising jumps in the spatial gradient of the solution at the physical boundary (Sticko *et al.*, 2020). These additional constraints stabilise the degrees of freedom associated with the smallest eigenvalues of the linear system and therefore introduce a bound on the condition number. The technique is widely used in the cut/non-matching mesh FEM literature but has received little attention in other areas of computational mechanics.
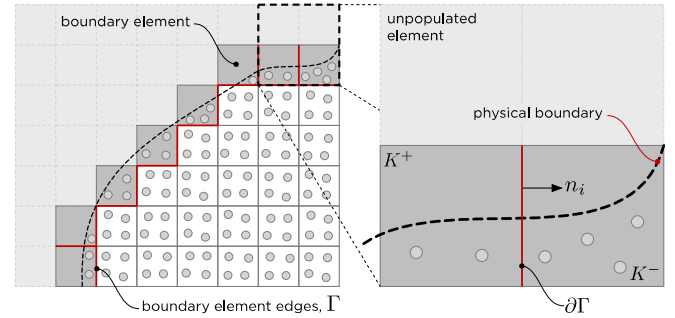

Figure 3. MPM boundary interpretation (reproduced from Coombs (2022))

An issue with applying the technique to the MPM is that most MPMs do not include an explicit presentation of the physical boundary of the problem domain. One way to approach this is to reconstruct the boundary of the computational domain using information about populated and unpopulated elements of the background grid, as shown in Figure 3. *Boundary elements* are defined as those elements that contain MPs but share a face with an unpopulated element. Ghost stabilisation can then be applied over the *boundary element edges* (Γ, red lines in Figure 3), defined as the boundary element faces shared with other populated elements.

3.1 Stiffness contribution and implicit solution

The additional stiffness associated with the ghost stabilisation term can be expressed as an integral over

the element faces of the background grid being cut by the boundary of the physical domain, Γ (see Figure 3). Assuming a background grid of bi-linear quadrilateral elements (see Coombs (2022) for details), the stiffness associated with the ghost stabilisation can be expressed as

$$[K_g] = \frac{\gamma_k h^3}{3} \int_{\Gamma} [G]^T [m][G] \, d\Gamma, \tag{2}$$

where γ_k is a stabilisation parameter, h is the size of the background grid face, $[G]$ contains spatial derivatives of the basis functions for the elements attached to the face under consideration

$$[G] = [[G^+] \quad -[G^-]]. \tag{3}$$

The superscripts denote the positive and negative elements (see Figure 3), with $[G^+]$ and $[G^-]$ sharing a common format. For example for 2D analysis

$$[G^+] = \begin{bmatrix} N_1^+,_x & 0 & \dots \\ 0 & N_1^+,_y & \dots \\ 0 & N_1^+,_x & \dots \\ N_1^+,_y & 0 & \dots \end{bmatrix}, \tag{4}$$

where N_i^+ are the basis functions of the positive element and the subscript 1 denotes the local node number. Finally, $[m] = [n][n]^T$ where for 2D analysis

$$[n]^T = \begin{bmatrix} n_x & 0 & 0 & n_y \\ 0 & n_y & n_x & 0 \end{bmatrix}, \tag{5}$$

n_x and n_y are the components of the vector normal to the boundary of the positive element (see Figure 3).

The appropriate value of the stabilisation parameter, γ_k, is a point of debate in the literature, with most authors suggesting that it should be related to the P-wave modulus of the material, such as $\gamma_k = (2\mu + \lambda) \cdot 10^{-4}$ (Hansbo *et al.*, 2017) where λ and μ are the Lame parameters. In the author's experience γ_k should be set to the minimum value that stabilises the analysis so that the stability terms do not onerously impact on the physical solution close to the boundary.

Although in general the spatial derivatives of the basis functions in $[G]$ and the normal direction to the element faces will depend on the incremental displacements within the current step, it is assumed that the ghost stabilisation contribution is constant over a given load/time step based on the configuration at the start of the step. This is reasonable as the exact value of the stabilisation contribution is arbitrary – the key contribution of the additional stiffness is to bound the lowest eigenvalue of the linear system being solved. It also allows the associated force contribution to the

equilibrium equations to be determined based on the incremental nodal displacements, $\{\Delta d\}$, via

$$\{f_g\} = [K_g]\{\Delta d\}. \tag{6}$$

This ghost force acts as an additional internal force contribution to the discretised weak form statement of equilibrium. Therefore, inclusion of the ghost stabilisation approach requires the ghost stiffness to be evaluated at Step 1 (see Section 2 for the key MPM steps) and then the current incremental nodal displacements to be used in Step 4 to determine the ghost force contribution.

4 NUMERICAL ANALYSIS

This section provides two analyses to demonstrate the ability of the ghost stabilisation approach to improve the robustness of the MPM for geotechnical analysis. The method was implemented within the AMPLE code of Coombs & Augarde (2020).

4.1 Compaction under self-weight

The first example considers the convergence behaviour of the elastic compression of a plane strain column with an initial height of $l_0 = 50$m under self-weight (shown on the right of Figure 4). The material had a Young's modulus of 10kPa and a Poisson's ratio of zero. The background was comprised of square bi-linear elements initially populated by a 2 by 2 equally spaced GIMPs. The mesh was constrained by roller boundary conditions on the left and right boundaries as well as the base. A body force per unit volume of $b = 800$N/m^3 was applied over 40 equal load steps, causing the physical body to compress by approximately half its original height. $\gamma_k = 10^{-2}E = 100$Pa for all analyses.
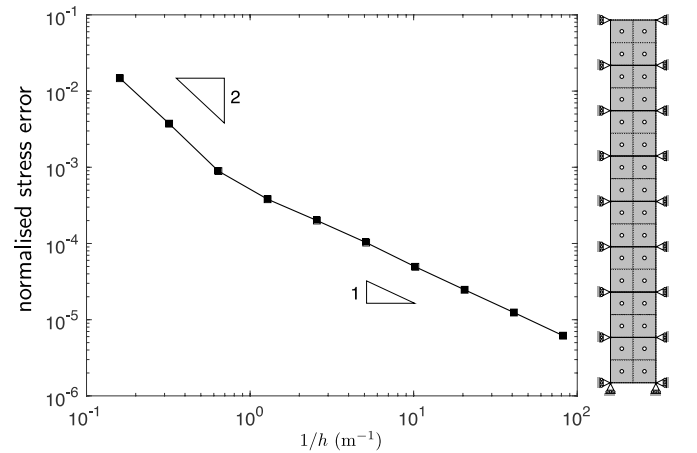

Figure 4. Column compression stress error

Figure 4 shows the normalised stress error convergence behaviour of the ghost-stabilised GIMPM

with background grid refinement. The error is defined as

$$\text{error} = \frac{1}{bl_0V}\sum_p \left|\sigma_{yy}^p - \sigma_{yy}^a\right|V_p \qquad (7)$$

where σ_{yy}^p and $\sigma_{yy}^a = b(l_0 - Y_p)$ are the numerical and analytical normal stress in the vertical direction at each MP, V_p is the original MP volume, $V = \sum_p V_p$ is the total original volume of the column, b is the imposed body force per unit volume and Y_p is the original vertical position of the MP.

The convergence rate is between linear and quadratic, which is consistent with the basis functions of the GIMPM method and the results available in the literature (for example see Charlton *et al.*, 2017) and is not degraded by the ghost stabilisation.

4.2 Slope failure

The second example considers the deformation of a 45 degree elasto-plastic plane strain slope due to gravitational loading. The geometry of the slope is shown in Figure 5, where: $A = (0,12)$m, $B = (10,12)$m, $C = (15,7)$m and $D = (30,7)$m. The material was represented by a linear elastic-perfectly plastic von Mises constitutive model with a Young's modulus of 1MPa, a Poisson's ratio of 0.3 and a von Mises yield strength of $\rho_y = 15$kPa. The yield function is defined as

$$f = \rho - \rho_y = 0, \qquad (8)$$

where $\rho = \sqrt{2J_2}$. J_2 is the second invariant of the deviatoric stress

$$J_2 = \frac{1}{2}tr([s][s]), \quad [s] = [\tau] - \frac{1}{3}tr([\tau]) \qquad (9)$$

and $[\tau]$ is the Kirchhoff stress. A weaker layer ($y \in [7,7.5]$m) was introduced in the model where the yield strength was reduced to of $\rho_y = 7.5$kPa, as shown by the light grey region in Figure 5. The material had a uniform initial density of 2,400kg/m³.
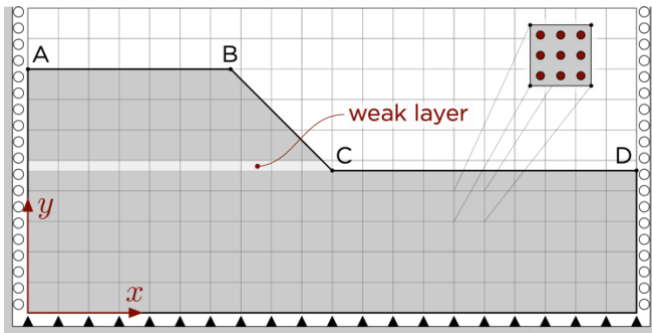

Figure 5. Slope geometry & boundary conditions

The slope was analysed with three different background grids, where $h = 1.0$, 0.5 and 0.25m, and three different generalised interpolation MP resolutions with 2^2, 3^2 and 4^2 equally spaced material points per background grid cell, giving a total number of MPs between 1,095 and 69,800. The physical geometry was defined by removing any material points outside of the slope geometry defined by points A through D in Figure 5. Gravitational loading of 9.81m/s² was applied over $40/h$ equal increments (load steps). The stabilisation parameter was initially set to $\gamma_k = 10^{-2}E = 10$kPa.

Table 1 provides the mean and maximum (in brackets) Newton-Raphson (NR) iterations for the standard GIMPM and the Ghost-Stabilised (GS) GIMPM for the analyses that were able to complete all of the load steps (indicated by the ✓). The unstable analyses are indicated by the ✗ and in those cases the final stable load step number is reported. The maximum permitted number of NR iterations was set to 20, with a normalised out of balance force residual tolerance of 10^{-6}.

Table 1. Mean and (maximum) number of NR iterations or final stable load step for unstable analyses

h (m)	1.0	0.5	0.25
2^2 MPs	✓ 5.50(7)	✗ 45	✓ 6.11(20)
3^2 MPs	✗ 23	✗ 56	✗ 57
4^2 MPs	✓ 5.48(6)	✓ 5.49(8)	✓ 5.83(8)
2^2 GSMPs	✓ 5.50(7)	✓ 5.55(7)	✓ 5.94(8)
3^2 GSMPs	✓ 5.48(6)	✓ 5.49(7)	✓ 5.85(8)
4^2 GSMPs	✓ 5.53(7)	✓ 5.48(7)	✓ 5.83(7)

Only 5 of the 9 standard GIMPM analyses were able to apply the full gravitational load and there is no obvious pattern of the grid/MP properties of the stable analyses. The other analyses failed to converge at a particular load step due to poor conditioning of the linear system of equations resulting in non-physical excessive displacements of the background grid and *numerical explosion* of the MPs. Note that one of the $h = 0.25$m, 4^2MPs/element load steps failed to satisfy the governing equations to 10^{-6} within the 20 load steps, however the analysis remained stable and all subsequent load steps converged. All the ghost-stabilised analyses were able to apply the full gravitational load, irrespective of the number of MPs and the size of the background grid.

Table 2. γ_k influence on the mean and (maximum) number of NR iterations for $h = 1$m and 3^2 MPs/element

γ_k/E	0	10^{-8}	10^{-6}	10^{-4}	10^{-2}
	✗	5.85(20)	5.50(7)	5.50(7)	5.48(6)

Table 2 the mean and maximum (in brackets) NR iterations for the ghost-stabilised GIMPM with $h = 1$m

and 3^2 MPs/element for different values of stabilisation parameter. The number of iterations is relative insensititve to the stabilisation parameter magnitude for $\gamma_k \geq 10^{-6}E$. Once the parameter reduces below this the analysis struggles to converge, reaching the maximum number of NR iterations for load step 24 when $\gamma_k = 10^{-8}E$ as this value is insufficient to stabilise the elements at the edge of the physical domain. The subsequent steps converge but with quesitonable validity as subsequent steps are based on the non-converged configuration.

Figures 6 and 7 show the deformed MPs at the end of the analysis shaded according to σ_{xy} for the standard GIMPM (Figure 6) and ghost-stabilised GIMPM (Figure 7) with $h = 0.25$m and 4^2MPs/element. The weaker layer is clearly visible in the shear stress distribution. The difference in the shear stress distribution between the standard and ghost-stabilised is most visible between along the slope (B to C, Figure 5), where the ghost stabilisation removes the stress oscillations seen in the standard GIMPM.
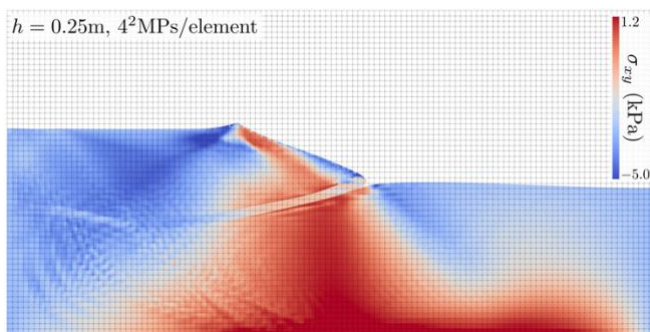

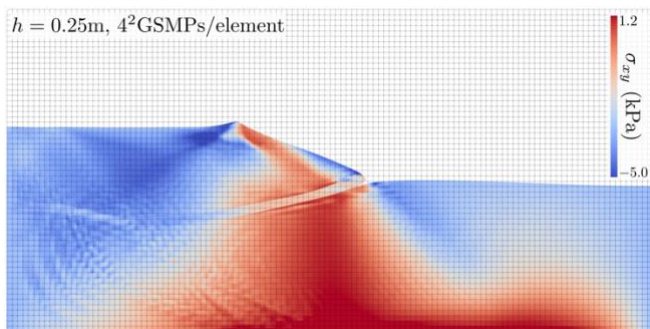*Figure 6. Deformed slope shaded by σ_{xy} for the standard GIMPM*

Figure 7. Deformed slope shaded by σ_{xy} for the ghost-stabilised GIMPM

5 CONCLUSIONS

This paper has presented a ghost-stabilised MPM applied to geotechnical analysis. The key advantage of the method is it introduces a bound on the conditioning of the linear system of equations solved as part of an implicit MPM solution algorithm. This significantly improves the stability of the method and removes much of the uncertainty regarding if a particular analysis will run or not based on the interactions between the MPs and the background grid. Without confidence in the stability of the method it is unlikely that the MPM will become a useful engineering tool for geotechnical analysis.

Although this paper has focused on implicit quasi-static analysis, the approach is equally applicable to explicit dynamic MPMs. In this case the mass matrix is stabilised in a similar way to the stiffness stabilisation detailed in this paper, see Coombs (2022) for details.

6 ACKNOWLEDGEMENTS

7 REFERENCES

Bardenhagen, S.G., Kober, E.M. 2004. The generalized interpolation material point method. *Computer Modeling in Engineering and Sciences* **5**: 477–495.

Burman E. 2010. Ghost penalty. *Comptes Rendus Mathematique* **348**(21): 1217-1220

Charlton, T.J., Coombs, W.M., Augarde, C.E. 2017. iGIMP: An implicit generalised interpolation material point method for large deformations. *Computers and Structures* **190**: 108-125.

Coombs, W.M., Augarde, C.E. 2020. AMPLE: A Material Point Learning Environment. *Advances in Engineering Software* **139**: 102748.

Coombs, W.M. 2022. Ghost stabilisation of the Material Point Method for stable quasi-static and dynamic analysis of large deformation problems. *ArXiv* 1-40.

Hansbo, P., Larson, M., Larsson, K. 2017. Cut Finite Element Methods for Linear Elasticity Problems. *Lecture Notes in Computational Science and Engineering* 25-63.

Sadeghirad, A., Brannon, R.M., Burghardt J. 2011. A convected particle domain interpolation technique to extend applicability of the material point method for problems involving massive deformations. *International Journal for Numerical Methods in Engineering* **86**(12): 1435–1456.

Sticko S, Ludvigsson G, Kreiss G. 2020. High-order cut finite elements for the elastic wave equation. *Advances in Computational Mathematics* **46:45**: 1-28.

Sulsky D, Chen Z, Schreyer HL. 1994. A particle method for history-dependent materials. *Computer Methods in Applied Mechanics and Engineering* **118**(1): 179–196.

Yamaguchi, Y., Moriguchi, S., Terada, K. 2021. Extended B-spline-based implicit material point method. *International Journal for Numerical Methods in Engineering* **122**(7): 1746-1769